

A dynamical study on the habitability of terrestrial exoplanets II: The super Earth HD 40307 g

R. Brasser¹, S. Ida² and E. Kokubo³

¹ *Institute for Astronomy and Astrophysics and Theoretical Institute for Advanced Research in Astrophysics, Academia Sinica, Taipei 10617, Taiwan*

² *Earth-Life Science Institute, Tokyo Institute of Technology, Ookayama, Meguro district, Tokyo 152-8551, Japan*

³ *Division of Theoretical Astronomy, National Astronomical Observatory of Japan, Osawa, Mitaka district, Tokyo 181-8588, Japan*

25 March 2014

ABSTRACT

HARPS and *Kepler* results indicate that half of solar-type stars host planets with periods $P < 100$ d and masses $M < 30 M_{\oplus}$. These super Earth systems are compact and dynamically cold. Here we investigate the stability of the super Earth system around the K-dwarf HD40307. It could host up to six planets, with one in the habitable zone. We analyse the system’s stability using numerical simulations from initial conditions within the observational uncertainties. The most stable solution deviates 3.1σ from the published value, with planets e and f not in resonance and planets b and c apsidally aligned. We study the habitability of the outer planet through the yearly-averaged insolation and black-body temperature at the pole. Both undergo large variations because of its high eccentricity and are much more intense than on Earth. The insolation variations are precession dominated with periods of 40 kyr and 102 kyr for precession and obliquity if the rotation period is 3 d. A rotation period of about 1.5 d could cause extreme obliquity variations because of capture in a Cassini state. For faster rotation rates the periods converge to 10 kyr and 20 kyr. The large uncertainty in the precession period does not change the overall outcome.

Key words: planets and satellites: general; planets and satellites: dynamical evolution and stability; planets and satellites: formation

1 INTRODUCTION

Since the discovery of the first extrasolar planet in 1995 (Mayor & Queloz, 1995) there has been a surge in research in planetary science and in the detection of new planets, with the HARPS survey (Mayor et al., 2003) and NASA’s *Kepler* mission leading the field. The high number of detected and candidate planets allows for statistical studies and several trends have emerged, which are shared among both the HARPS and *Kepler* data (Figuera et al., 2012). Some of these include:

- Approximately half of all solar-type stars contain planets with a projected mass $m_p \sin I < 30$ Earth masses (M_{\oplus}) (Borucki et al., 2011; Mayor et al., 2011; Chiang & Laughlin, 2013), where m_p is the planet’s mass, and I is the angle between the planet’s orbit and the observer.
- Planets with a short orbital period tend to be of low ($< 30 M_{\oplus}$) mass (Mayor et al., 2011; Batalha et al., 2013). Most of these have radii $R \in [1, 4]$ Earth radii (R_{\oplus}) and masses between Earth’s and Neptune’s. These planets are often referred to as super Earths. In contrast, hot Jupiters are rare (Mayor et al., 2011).
- The number of planets increases with decreasing mass and/or radius (Howard et al., 2010; Howard et al., 2012) and approxi-

mately 23% of stars have Earth-like close-in planets with periods $P < 50$ days (d).

- Approximately 73% of low-mass planets with periods shorter than 100 d reside in multiple systems (Mayor et al., 2011; Fang & Margot, 2012), with only 26% of these multiples containing a gas giant (Mayor et al., 2011). This suggests that super Earths form in clusters close to the parent star and are isolated from potential giant planets in the system.

- Systems of multiple super Earths on short periods tend to be compact (Fang & Margot, 2012; Chiang & Laughlin, 2013) and have low ($< 3^\circ$) mutual inclinations (Fang & Margot, 2012; Tremaine & Dong, 2012) and most likely also low (< 0.2) eccentricities (Mayor et al., 2011; Wu & Lithwick, 2013).

- The period distribution is more or less random with some excesses just slight of the 3:2 and 2:1 mean motion resonances (Fabrycky et al., 2012). The near-resonance of some pairs has been attributed to tidal decay (Batygin & Morbidelli, 2013; Lithwick & Wu, 2012), though Petrovitch et al. (2013) proposed an alternative scenario based on planet growth.

- Although still actively debated, the period distribution of exoplanets with short ($P < 200$ d) periods suggests an in-situ formation scenario (Raymond et al., 2008; Hansen & Murray, 2012; Chiang & Laughlin, 2013) rather than formation farther out fol-

lowed by migration (Lopez et al., 2012; Kley & Nelson, 2012; Rein, 2012). An intermediate scenario in which planetary embryos migrate inwards followed by a giant impact stage (Ida & Lin, 2010) may also work.

- The mutual spacing of most of these super Earths is between 5 to 30 Hill radii (Lissauer et al., 2011; Fabrycky et al., 2012), which encompasses the spacing between the giant planets (12) and terrestrial planets (40). However, their proximity to the star requires their orbits to be dynamically cold to prevent orbit crossing.

- The Kepler catalogue contains a few confirmed super Earth planets in the habitable zone of their parent stars, with a further 20 candidates (Batalha et al., 2013). The habitable zone (HZ) is the region where radiation received by the planet from the star is enough for it to sustain liquid water under sufficient atmospheric pressure (Kasting et al., 1993; Kaltenegger & Sasselov, 2011).

Thus, it seems the super Earth population resembles the regular satellite populations of the giant planets: both show a typical mass ratio of $m_p/M_* \sim 10^{-4.5}$ and regularly spaced, dynamically cold orbits. Some are far enough out to be in the habitable zone.

The regularity of the orbits and tight spacing provide a formidable challenge to theorists of planet formation and dynamicists alike. If the best determined orbits are not entirely circular determining whether or not these systems are dynamically stable and fall within the observational uncertainties is challenging. The aim of this study is to analyse the stability of one such compact super Earth system: HD 40307. This system is interesting because one planet, HD 40307 g, may be in the habitable zone. Therefore we also study how the dynamics of the whole system affects the long-term habitability of planet g.

The term ‘habitable’ encompasses many things, however, thus we only focus on the long-term variations in the insolation caused by the dynamics of the whole system and the solid body response of planet g. On Earth, in addition to stellar activity, geological activity and temperature regulation through the carbonate-silicate cycle (Williams & Kasting, 1997), the long-term climate is driven externally by the Milanković cycles (Milanković, 1941). Earth’s orbit is perturbed by other planets, causing quasi-periodic variations in eccentricity and inclination on a time scale of 100 kyr. The Earth’s obliquity is also affected and oscillates on a time scale of 41 kyr (e.g. Laskar et al., 1993). The combined effect of the variations in eccentricity, obliquity and precession angle are the Milanković cycles. Those periods of the Milanković cycles are much shorter than the relaxation time of the carbonate-silicate feedback mechanism. The perturbations of other planets cause these changes and so influence the insolation accordingly, driving the ice ages on the Earth (Imbrie & Imbrie, 1980). Small variations in eccentricity and obliquity most likely yield stable and favourable conditions for habitability (Atobe et al., 2004; Brasser et al., 2013).

We want to know what are the dynamical properties of close super Earth systems and how dynamics affects the habitability of potentially habitable planets. This paper is a proof of concept on how to determine the dynamical stability of a compact super Earth system, and how the long-term insolation variation of any planets in the habitable zone depends on the dynamics of the whole system. Other effects, such as a general circulation model (GCM) of the planet, and affects of atmospheric heat transport and buffering, ice-albedo feedback, carbon dioxide cloud formation, are not a part of this study but will be part of future projects.

This paper is organised as follows. The next section contains an overview of the HD 40307 planetary system. In Section 3 we describe our numerical methods. In Section 4 we summarise the the-

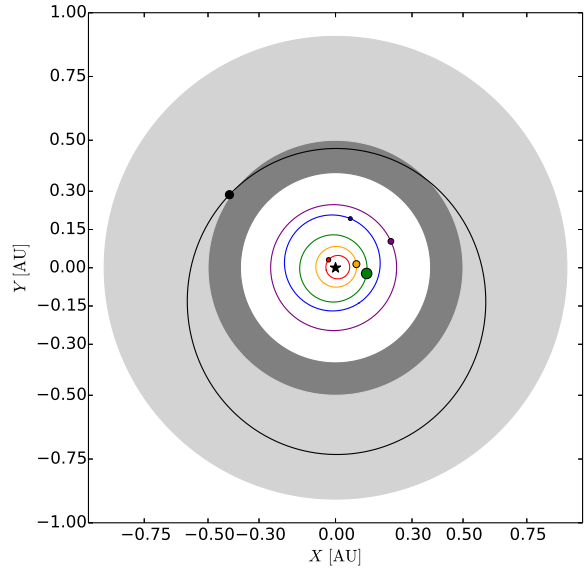


Figure 1. A top-down view of the orbits of the planets orbiting HD 40307 drawn to scale. The positive x -axis marks zero longitude. The shaded area marks the habitable zone. The positions of the planets are taken from Table 1. The planets’ marker sizes are proportional to their masses.

ory of how orbital perturbations affect the obliquity and the black-body equilibrium temperature of the planet. This is followed by our results in Section 5. Section 6 focuses on the long-term climate cycles and Section 7 is reserved for a discussion. We present a summary and conclusions in Section 8.

2 SYSTEM OVERVIEW

From high resolution spectroscopic data with the HARPS instrument at ESO’s 3.6 m telescope at La Silla, the K-dwarf star HD 40307 was found to have three planetary companions on near-circular orbits with periods ranging from 4 d to 20 d and masses from 4 to 10 Earth masses on dynamically stable orbits (Mayor et al., 2009). A subsequent re-analysis of the data with the HARPS-TERRA algorithm (Anglada-Escude & Butler, 2012) and the inclusion of further observations led Tuomi et al. (2013) to conclude that HD 40307 may be surrounded by up to six super Earth planets, with the outermost one being in the habitable zone. Figure 1 shows a top-down view of the orbits of the HD 40307 system, using the orbital parameters of Tuomi et al. (2013). The star is surrounded by a compact inner five-planet system of super Earths and a last planet farther out in the habitable zone on a fairly eccentric orbit. The habitable zone is indicated by light grey shading. In this paper we analyse the dynamical stability of the system and the obliquity and insolation forcing on planet g. In order to do so we need a dynamically stable solution that best matches the HARPS data. However, when fitting the orbital solution of Tuomi et al. (2013) to the radial velocity data, we computed a reduced $\chi^2 \gg 10$, indicating a poor fit and casting doubt on the published solution. We attempted to reduce it and still be consistent with the radial velocity data. The radial velocity at any epoch is given by

Table 1. Orbital element solution of the HD 40307 system from Tuomi et al. (2013) with updated mean longitudes. We list the means and standard deviations, whenever available, taken both from their tables and figures. When two values are listed in the square brackets these correspond to minimum and maximum values respectively. Unlike Tuomi et al. (2013) we did not consider variations in the mass of the star and thus our deviations in the semi-major axis are smaller than theirs. The equilibrium temperatures are computed by us. The value in brackets is the orbit-averaged value where the nominal eccentricity was used. We have taken the albedos to be 0.3, the stellar surface temperature was $T_* = 4700$ K and the stellar radius was $0.91 R_\odot$ and its luminosity is $L = 0.23 L_\odot$.

Parameter ($\mu, [\sigma]$)	HD 40307 b	HD 40307 c	HD 40307 d
P [days]	4.3123 [3.9167×10^{-4}]	9.6183 [1.6825×10^{-3}]	20.4321 [7.5606×10^{-3}]
e	0.1964 [0.054187]	0.05777 [0.03609]	0.06728 [0.03514]
ω [$^\circ$]	194.8 [137.5, 240.6]	234.9 [-]	17.2 [-]
λ [$^\circ$]	150.0 [-]	5.0 [-]	353.0 [-]
$m_p \sin I$ [M_\oplus]	4.0 [3.3, 4.8]	6.6 [5.6, 7.7]	9.5 [8.0, 11.2]
a [AU]	0.047524 [3×10^{-6}]	0.08113 [2×10^{-5}]	0.13407 [3×10^{-5}]
$\langle T_{eq} \rangle$ [K]	910 [1217]	696 [792]	541 [625]
	HD 40307 e	HD 40307 f	HD 40307 g
P [days]	34.6279 [6.9005×10^{-2}]	51.7768 [0.1721]	196.343 [2.1817]
e	0.1201 [0.06653]	0.06175 [0.04534]	0.2205 [0.1113]
ω [$^\circ$]	303.7 [-]	355.2 [-]	91.7 [-]
λ [$^\circ$]	62.0 [-]	308.0 [-]	127.0 [-]
$m_p \sin I$ [M_\oplus]	3.5 [2.1, 4.9]	5.2 [3.6, 6.7]	7.1 [4.5, 9.7]
a [AU]	0.1906 [2×10^{-4}]	0.2491 [6×10^{-4}]	0.6069 [9.6×10^{-4}]
$\langle T_{eq} \rangle$ [K]	455 [558]	398 [423]	255 [349]
$\chi^2 = 2.5$	JD 2450000		

$$V_r = V_0 + \sum_{k=1}^6 \frac{m_k}{M_*} \frac{2\pi a_k}{P_k} \frac{\sin I}{\sqrt{1-e_k^2}} [\cos(v_k + \omega_k) + e_k \cos \omega_k], (1)$$

where v_k is the planet's true anomaly, ω_k is its argument of periastron, a_k is the semi-major axis, P_k is the orbital period, m_k is the planetary mass, M_* is the stellar mass, I is the inclination of the orbital plane with respect to the viewer and V_0 is a non-zero drift velocity. Apart from the periods, the greatest variation in V_r is caused by changing $v_k + \omega_r$, and thus we used a simple grid search, varying the initial mean longitude of each planet, until we found the minimum $\chi^2 = 2.5$. The orbital elements corresponding to this minimum are given in Table 1. We list the mean values (μ) and standard deviations (σ), whenever available, of the following quantities: the orbital period, P , eccentricity, e , argument of periastron, ω , mean longitude at the epoch, λ , inferred planetary masses $m_p \sin I$, and semi-major axes, a . The semi-major axes are computed directly from the period and the standard deviations assume a Gaussian fit (Tuomi et al., 2013).

To obtain an overview of the system, we use some of the quantities introduced by Chambers (2001): the Angular Momentum Deficit (AMD) (Laskar, 1997), fraction of total mass in the most massive planet (S_m), a spacing parameter (S_s) that scales as the planet to star mass ratio $\mu^{1/4}$ rather than the Hill relation of $\mu^{1/3}$ (Chambers et al., 1996), and a concentration parameter (S_c) which measures how much mass is concentrated in a narrow annulus. We supplement this with listing the average spacing in Hill radii (S_H). We calculated these values for the entire system, the inner five planets, the terrestrial planets and the giant planets of our Solar System in Table 2.

The AMD of HD 40307 is about a factor five higher than either the terrestrial planets and giant planets of the Solar System. This is dominated by the high eccentricity of planets b and g. Systems with higher AMD are possibly more chaotic (Laskar, 1997) and have more opportunity to exchange it among the planets, resulting in larger eccentricity oscillations. However, due to the large spacing between planet g and the innermost planets, secular interaction

System	AMD	S_m	S_s	S_c	S_H
HD 40307	9.9×10^{-3}	0.265	21.7	8.29	19.6
HD 40307 b-f	2.1×10^{-3}	0.330	19.1	18.7	16.3
MVEM	1.8×10^{-3}	0.509	37.7	89.9	43.2
JSUN	1.3×10^{-3}	0.715	11.5	27.0	12.0

Table 2. Chambers' (2001) stability quantities for the entire HD 40307 system, the inner five planets, and for comparison also the terrestrial planets and giant planets of our Solar System.

Period ratio	Value (median; standard deviation)
P_c/P_b	2.2304 [5×10^{-4}]
P_d/P_c	2.1243 [4×10^{-4}]
P_e/P_d	1.6948 [3×10^{-3}]
P_f/P_e	1.4952 [6×10^{-3}]

Table 3. Period ratios between some inner planet pairs. Only the planets e and f appear to be in a resonance.

between these two groups will be minimal.

Given that all planets have comparable mass, S_m is lower than in the Solar System. The spacing parameter is comparable to that of the giant planets. However, the mass concentration parameter, S_c is the opposite: it is only of the order of 10, while in the Solar System's it ranges from 27 to 90. The low value of S_c indicates that all planets have a comparable mass and that the total mass is spread over a wide annulus rather than concentrated in a narrow one composed of two heavy planets.

We also inspect the period ratios between the planets for mean-motion resonances. These are listed in Table 3. The planets e and f appear close to a 3:2 mean motion resonance. Tuomi et al. (2013) concluded that the planets e and f need to be in a 3:2 resonance to be dynamically stable. The other planets do not appear to be in resonance, but Papaloizou & Terquem (2010) state that they are close

enough for their dynamics to be affected as if they were in resonance.

Another feature warranting discussion is the relatively high eccentricity of planet b. One would expect that its proximity to the star would have fully damped its eccentricity due to tidal effects. However, as shown by Lovis et al. (2011) and subsequently detailed by Batygin & Laughlin (2011), tidal eccentricity damping is more complicated than simply reducing the eccentricity to zero. Tidal friction damps the free eccentricity mode of planet b (mode 1) the fastest; the damping of the other (forced) modes takes much longer. Thus, it is most likely that the eccentricity of planet b is caused entirely by forcing from the other planets, mostly from planet c. Batygin & Laughlin (2011) demonstrate that in a two-planet system the complete damping of the mode corresponding to the innermost planet leads to apsidal alignment or anti-alignment of the two planets with the eccentricities in both planets having a fixed ratio; the actual configuration depends on the relative magnitudes of the two eigenfrequencies.

We can predict the configuration of the innermost two planets from theory. The tidal damping time scale of the eccentricity of the innermost planet can be obtained from Ferraz-Mello’s (2013) equilibrium tidal theory. For a quasi-stationary rotation in which the semi-diurnal forcing frequency, $f = 2\nu - 2n$, is low and $O(e^2)$, we have

$$\tau_{\text{eb}} = \frac{32}{1125} \frac{m_b R_b^2}{\mathcal{C}} \frac{m_b}{M_*} \left(\frac{a}{R_b} \right)^5 \left(1 + \frac{\gamma^2}{n^2} \right) \left(\frac{\gamma}{1 \text{ rad yr}^{-1}} \right)^{-1}, \quad (2)$$

where ν is the planet’s rotation frequency, $n = \sqrt{GM_*/a^3}$ the mean motion, \mathcal{C} the largest moment of inertia, M_* the stellar mass, a the semi-major axis, m_b and R_b are the mass and radius of planet b and γ is the tidal relaxation frequency. If we assume that $\gamma \sim 1.8 \times 10^{-7} \text{ Hz}$ ($\sim 35.7 \text{ rad yr}^{-1}$) as for solid Earth and that the planet follows the mass-radius relation $R_b/R_\oplus \sim (m_b/m_\oplus)^{0.274}$ (Valencia et al., 2006; Sotin et al., 2007), which appears consistent with observations of super Earth planets (Gaidos et al., 2012), we have $\tau_{\text{eb}} \sim 10 \text{ Myr}$. Thus the eccentricity associated with mode 1 should be fully damped in approximately $\sim 50 \text{ Myr}$, much shorter than the age of the system. This value is uncertain by a factor of a few, with the largest uncertainty coming from the estimate of the planetary radius. This short eccentricity damping time scale is somewhat problematic because over the course of several Gyr the corresponding tidal decay of the semi-major axis is $\sim 0.02 \text{ AU}$ assuming $e \sim 0.1$. This poses constraints on the formation and past evolution of the system that are beyond the scope of this paper.

The eccentricity mode corresponding to planet c will decay on a time scale of at least $\tau_{\text{ec}} \sim 200 \text{ Myr}$, so that this mode may have also decayed since the formation of the system. However, given the uncertainty in γ it is not evident that the mode corresponding to planet c has also decayed away. We have used γ for the solid Earth because the size of the planets suggest they may be partially molten inside. But when setting γ equal to the values for Mars and the Moon, which are practically solid bodies, the decay times become one to two orders of magnitude longer: still short enough to damp the eigenmode corresponding to planet b but not that of planet c.

Unfortunately planets e and f could be in a 3:2 resonance so that the often-used Laplace-Lagrange theory cannot accurately predict their apsidal precession frequencies. Nevertheless, we applied the theory to the nominal orbital elements of the system and computed the eigenfrequencies. We used the modified AMD Laplace-Lagrange theory from Agnor & Lin (2012), which gives a better overview of the amount of AMD in each eigenmode.

$g_1 ['' \text{ yr}^{-1}]$	g_2	g_3	g_4	g_5	g_6
1834	1018	232	1541	561	16.7
$s_1 ['' \text{ yr}^{-1}]$	s_2		s_4	s_5	s_6
-2036	-1002	0.0	-1615	-488	-25.5

Table 4. Eigenfrequencies g_n and s_n of the HD 40307 planetary system obtained using the Laplace-Lagrange AMD theory of Agnor & Lin (2012). The frequencies depend on the original configuration of the orbits i.e. the frequencies increase if planets are more eccentric and thus spend more time in each other’s presence, or if orbits are nearly anti-aligned versus being aligned.

j/i	1	2	$S_{i,j}$ 3	4	5	6
1	0.5311	-0.6678	0.1451	0.3469	-0.3641	0.0024
2	-0.7126	-0.3643	0.2669	-0.2282	-0.4860	0.0050
3	0.3699	0.5103	0.5021	-0.3158	-0.5008	0.0133
4	-0.2659	0.3019	0.4066	0.8202	0.0018	0.0157
5	0.0507	-0.2641	0.6997	-0.2348	0.6184	0.0242
6	-0.00003	0.00054	-0.02903	0.0001	-0.0060	0.9996

C_j^2	0.01701	0.1285	0.03871	0.03999	0.01071	0.7650
β_j	118.6°	10.1°	320.7°	253.9°	23.1°	91.4°

Table 5. Eccentricity eigenvectors (columns) of the Laplace-Lagrange AMD solution (Agnor & Lin, 2012) for the nominal orbital parameters listed in Table 1. The rows depict the forcing of the planets on each other. The integration constants (amplitude and phases) are listed separately in the bottom.

We included the effect of General Relativity following Batygin & Laughlin (2011). We did not include the influence of tides or additional effects arising from the non-spherical shape of the planets because these are all insignificant compared to General Relativity (Batygin & Laughlin, 2011). We listed the eccentricity (g_i) and inclination (s_i) eigenfrequencies in Table 4. Unlike in the Solar System, the strong coupling between the inner five planets makes identification of any frequency with a particular planet rather difficult and the identification that is listed is a result of numerical simulations. The corresponding eccentricity eigenvectors, with components $S_{i,j}$, are listed as the columns of Table 5, with the normalised integration constants C_j^2/AMD (Agnor & Lin, 2012), β_j (amplitudes and phases) given separately below. The rows identify the strength of the forcing on a particular planet caused by the other planets. The total entropy is $Z \equiv -\sum_{j=1}^{2N-1} C_j^2 \ln C_j^2$ (Wu & Lithwick, 2011), which evaluates to $\exp(Z) \sim 2.3$ out of a maximum of 11. The minimum value of Z is 0, corresponding to the AMD being confined to one single eigenmode, while Z approaches $\ln 11$ at equipartition. The fairly low value of Z suggests that the AMD is confined to two eigenmodes (modes 2 and 6) and the system has undergone some AMD diffusion in the past. Since we consider a planar system only, the value of Z is most likely to be higher. For the inner five planets only $\exp(Z) \sim 3.5$ and three eigenmodes are activated (modes 2, 3 and 4). From the top row of Table 5 one may see that the eccentricity of planet b contains strong forcing from all eigenmodes, but mostly from mode 2. Thus it is not surprising that planet b has a fairly high eccentricity. Assuming that this eccentricity is mostly a forced component from mode 2, and numerical

simulations demonstrate that the eccentricity of planet c is aligned with eigenmode 2, then the planets b and c are likely to reside in apsidal alignment. Indeed, the components $S_{2,1}$ and $S_{2,2}$ carry the same sign and $g_1 > g_2$ so that the nominal solution of Table 1 places planets b and c in apsidal alignment.

Note also that $C_2^2 \gg C_{1,3,4,5}^2$ which begs the question whether the excitement of eigenmode 2 is a remnant of formation, of chaotic AMD diffusion or caused by a past 2:1 resonance passage with planet b as the latter spirals towards the star by tidal interaction. If it is the latter this passage should have occurred recently because the eccentricity in planet c will decay away on a time scale of $O(1 \text{ Gyr})$.

3 NUMERICAL METHODS

We analysed the stability of the HD 40307 system with a high number of numerical simulations. Our procedure was as follows.

First, we generated a new set of orbital parameters within the observational uncertainties, restricting ourselves to the deviations in the orbital periods, eccentricities and arguments of periastron. We assumed the latter were evenly distributed from 0 to 360° . We kept the mean longitude constant and equal to their nominal values.

We sampled the semi-major axis or eccentricity evenly between -3σ and 3σ . This procedure was repeated a second time for another orbital element resulting in an evenly-spaced 2-dimensional grid in $a-e$, $a-\omega$ or $e-\omega$. For each set of simulations we only changed the orbital elements of a single planet, keeping the orbital elements of the others at their nominal values. A typical grid contained 12 000 entries.

Second, we integrated the system and analysed its stability in a manner similar to Correia et al. (2005). We simulated each fictitious system for 40 kyr using the integrator SWIFT MVS (Levison & Duncan, 1994), which is based on the fast and reliable Wisdom-Holman method (Wisdom & Holman, 1991). General relativity was included by adding the effect of a perturbing potential that yields the correct periastron precession (Nobili & Roxburgh, 1986), but does not reproduce the increased orbital frequency (Saha & Tremaine, 1994). This potential is

$$V_{\text{GR}} = -3 \left(\frac{GM_*}{c} \right)^2 \frac{a}{r^3}, \quad (3)$$

where G is the gravitational constant, M_* is the stellar mass, c is the speed of light and r is the planet-star distance. The time step was set to $3 \times 10^{-4} \text{ yr}$ or 2.6 h, approximately 40 steps for the innermost planet's orbit. Output was generated every 40 yr. The simulation was stopped once a planet was farther than 1 AU from the star or once two planets entered each other's Hill spheres. SWIFT MVS cannot handle close approaches between the planets when they are closer than their mutual Hill spheres, and thus some simulations ended prematurely when such an encounter occurred. Our simulation time was motivated by the following argument. When two planets are on planar crossing orbits, the probability of the planets having an encounter within their Hill spheres is of the order of $(\frac{R_H}{\pi a})^2$, where $R_H = a(m_p/3M_*)^{1/3}$ is the size of the Hill sphere of each planet. For this system typically $m_p/M_* \sim 2 \times 10^{-5}$ and thus the encounter probability is $P_{\text{enc}} \sim 4 \times 10^{-5}$. Hence the time between encounters is $P_{\text{enc}}^{-1} \sim 20 \text{ kyr}$ and thus most unstable configurations should be detected within this time. We ran some test simulations for 20 kyr and 40 kyr and concluded that the latter resulted in more reliable stability maps. Thus we ran for 40 kyr.

We analysed the stability using a variant of Laskar's frequency

analysis method (Laskar, 1993). The advantage of the frequency analysis method is that it does not require long-term simulations and thus large regions of phase space can be tested in a reasonably short time. Frequency analysis relies on computing a diffusion index, D , which is the fractional difference of the orbital frequency of a planet averaged over two consecutive time intervals whose total time is the simulation time i.e. $T_1 = T_2 = T/2$. Therefore $D = |n_1 - n_2|$, where n_1 is the orbital frequency measured during the first interval, and n_2 is the orbital frequency during the second interval. However, while frequency analysis has been applied to study the stability of many systems it often does not determine stability directly because the integrations are too short for the planets to have encounters and for the system to relax. As a result, some long-term stable trajectories may be flagged as chaotic over short durations.

We decided to approximate the orbital frequencies with the averaged mean motions over each interval using Kepler's third law and follow the procedure of Marzari et al. (2003). We compute the average of the mean motion $\langle n_i \rangle$ over N time intervals each of length $T_i = T/N$ and then compute the standard deviation, σ_n , over these N intervals. The stability index is then given by $D = \log(\sigma_n/n_{\text{orig}})$, where n_{orig} is the original mean motion that corresponds to the published orbital period. We tested the procedure with five, ten and twenty intervals and concluded that twenty intervals resulted in the best stability map. We did not perform any tests with more intervals.

We realise that the interpretation of our method is not the same as with the frequency analysis. The latter measures diffusion in the frequency space, while our method considers diffusion in action space through the relation between n and a . Although for regular motion the frequencies are constant and well defined, the actions such as the semi-major axis usually undergo small oscillations so that in theory it is not adapted for diffusion measurements. However, in practise the average semi-major axis, being an action of the Hamiltonian, is approximately constant along regular trajectories and its standard deviation could be a proxy for chaos and thus for instability. We repeat that here we are interested in determining the stability of the system rather than whether or not it is chaotic. The stability is compromised by planetary encounters. The value of D is directly related to the strength of a planetary encounter, and very close encounters just outside the Hill sphere can lead to high values of D , much higher than the deviations caused by approximating the mean motion with the orbital frequency. Thus our procedure is justified.

In addition to obtaining the index D we also compute $D_{\text{max}} = \max(D_j)$ i.e. the maximum value of all six D -values of the planets. Low values ($D_{\text{max}} \lesssim -3$) correspond to a quasi-stable solution while high values ($D_{\text{max}} \gtrsim -2$) are synonymous with unstable motion. When the simulation did not reach the final time because of a close encounter we arbitrarily set $D_{\text{max}} = 0$.

We also compared the orbital configurations with the radial velocity data using the methods of Beaugé et al. (2012). For each pair of elements in the stability map we calculated the radial velocity of HD 40307 at each epoch for which data was available. We test the goodness of fit of the orbital elements to the radial velocity data using the reduced χ^2 . The radial velocity data used here is the same as that of Tuomi et al. (2013) and contains the same error sources. However, as discussed in Beaugé et al. (2012), care should be taken in blindly using χ^2 because it assumes the errors are normally distributed, which is often not the case. However, for want of a better descriptor, we employ it here with this caveat in mind.

Once one set of simulations was completed, we determined which initial values of orbital elements yielded the most stable system that best agreed with the radial velocity data. We then updated the initial orbital elements of the planet whose orbital elements were varied with those that gave the most stable configuration. We then used these updated elements for the next set of simulations. This semi-iterative procedure ensures that each successive set of simulations has a high probability of converging to a stable solution while still residing within the observational uncertainties. The above steps are repeated until we have found a sizeable region of phase space where the system could be stable. We simulate the most stable configuration for 1 Myr to determine its longer-term stability and use its output to determine the long-term climate cycles of planet g below. All simulations were performed on the HTCCondor pool at the Institute for Astronomy and Astrophysics, Academia Sinica.

4 BASIC THEORY OF HOW ORBITAL DEVIATIONS AFFECT LONG-TERM CLIMATE TRENDS

In this section we summarise how long-period orbital variations in a planet's orbit can affect the insolation on long time scales. We shall discuss the case on Earth first since this is the best-studied example and then summarise how these effects could apply to planet g.

It has been suggested that the long-term stability of the Earth's climate is related to the Milanković cycles (Milanković, 1941), which cause insolation variations on long time scales due to changes in the Earth's eccentricity, obliquity and precession angle. These variations manifest themselves the most at high latitudes. The onset and disappearance of ice ages appear correlated to the insolation at summer solstice rather than the yearly-averaged insolation (Imbrie, 1982; Huybers, 2011). Each of these three perturbations cause insolation forcing with specific periods of 100 kyr for the eccentricity, 41 kyr for the obliquity and 23 kyr for the precession. The recent Pleistocene ice ages record appears to be paced by both obliquity and precession forcing (e.g. Huybers & Wunsch, 2005; Huybers, 2011; Abe-Ouchi et al., 2013). To determine the insolation changes on planet g, we need to know how its obliquity and insolation change with time.

Introducing $\chi = \xi + \eta = \sin \varepsilon \exp(i\psi)$, where ε is the obliquity of the planet, ψ is the node of the planet's equator with its orbit (the precession angle) and i is the imaginary unit, the equations of motion of a planet's obliquity variations caused by perturbations from other planets on its orbit are (Neron de Surgy & Laskar, 1997)

$$\begin{aligned}\dot{\xi} &= A(t)\sqrt{1-\xi^2-\eta^2} - \eta[\alpha\sqrt{1-\xi^2-\eta^2} - 2\Gamma(t)], \\ \dot{\eta} &= -B(t)\sqrt{1-\xi^2-\eta^2} + \xi[\alpha\sqrt{1-\xi^2-\eta^2} - 2\Gamma(t)].\end{aligned}\quad (4)$$

We have

$$\begin{aligned}\Gamma(t) &= \dot{p}q - \dot{q}p, \\ A(t) &= 2\frac{\dot{q} + p\Gamma(t)}{\sqrt{1-p^2-q^2}}, \\ B(t) &= 2\frac{\dot{p} - q\Gamma(t)}{\sqrt{1-p^2-q^2}},\end{aligned}\quad (5)$$

with $\zeta = q + ip = \sin(\frac{i}{2}) \exp(i\Omega)$. Here i is the inclination of the orbit of a planet with respect to the invariable plane of the planetary system and Ω is its longitude of the ascending node from an

arbitrary reference direction. We also have the precession constant of the planet's equator

$$\alpha = \frac{3n^2}{2\nu} J_2 \left(\frac{m_p R_p^2}{C} \right) (1-e^2)^{-3/2}. \quad (6)$$

Here J_2 is the planet's quadrupole moment. The value of α depends on the quadrupole moment J_2 and the rotation rate. However, J_2 also depends on the rotation rate (e.g. Atobe & Ida, 2007) so that $\alpha \propto \nu$ and thus planets with longer spin periods have longer precession periods.

On Earth, the three forcing periods of the Milanković cycles are 100 kyr, 41 kyr and 23 kyr, caused by the superposition of the Earth's precession and the eigenfrequencies of the Solar System. We shall briefly discuss the origin of each of these frequencies and apply this knowledge to predict what these frequencies should be for planet g.

To lowest order, the variations in the Earth's eccentricity and longitude of perihelion, ϖ , can be Fourier decomposed as (e.g. Laskar, 1988)

$$e \exp(i\varpi) = \sum_{n=1}^N M_{n,3} \exp[i(g_n t + \beta_n)], \quad (7)$$

where g_n are the eccentricity eigenfrequencies of the Solar System (Brouwer & Van Woerkom, 1950), $M_{n,3}$ are the forcing amplitudes in the Earth and β_n are the corresponding phases.

A similar decomposition can be applied for the inclination and longitude of the ascending node

$$\sin(\frac{i}{2}) \exp(i\Omega) = \sum_{n=1}^N N_{n,3} \exp[i(s_n t + \delta_n)], \quad (8)$$

where s_n are the inclination eigenfrequencies with forcing amplitudes $N_{n,3}$ and phases δ_n . For the Earth, the largest eccentricity terms are in order $M_{5,3}$, $M_{2,3}$ and $M_{4,3}$ i.e. the terms associated with perturbations from Jupiter, Venus and Mars (Laskar, 1988). Their frequencies are $g_5 = 4.25''/\text{yr}$, $g_2 = 7.45''/\text{yr}$ and $g_4 = 17.78''/\text{yr}$ (Laskar, 1988). The superposition of these terms results in the eccentricity oscillating with three distinct frequencies which are $|g_5 - g_2|$ and $|g_4 - g_5|$ and $|g_4 - g_2|$; the corresponding periods are approximately 400 kyr, 128 kyr and 95 kyr respectively. The last two combine to form the 100 kyr eccentricity contribution (e.g. McGehee & Lehman, 2012). For the inclination, the dominant forcing is caused by Earth's eigenfrequency ($s_3 = -18.85''/\text{yr}$), Mercury ($s_1 = -5.57''/\text{yr}$) and Mars ($s_4 = -17.87''/\text{yr}$). This leads to periods of 1.2 Myr, 106 kyr and 98 kyr.

We can also apply the same principle to the variations in the obliquity and precession angle, which becomes (Laskar et al., 1993)

$$\sin \varepsilon \exp(i\psi) = \sum_{n=1}^N P_n \exp[i(\kappa_n t + \varsigma_n)]. \quad (9)$$

From this decomposition it turns out that κ_1 is the free precession frequency of the Earth's equator and is equal to $\dot{\psi}_{\oplus} = -50.29''/\text{yr}$ (Laskar et al., 1993), with corresponding period 25.8 kyr. Now $P_1 \gg P_{n>1}$, where $P_1 \sim 0.399$ corresponds to the Earth's mean obliquity of 23.5° . The second term has a forcing frequency $\kappa_2 = s_3 = -18.85''/\text{yr}$, the inclination eigenfrequency of the Earth. Thus the obliquity will predominantly oscillate about a mean of 23.5° with a frequency $|\dot{\psi}_{\oplus} - s_3|$, whose period is 41.2 kyr.

The last quantity in the Milanković cycles is the precession. The Earth's equator regresses about a fixed reference frame at a rate of approximately $50''/\text{yr}$. Summer solstice occurs when the declination of the Sun, δ_{\odot} , is highest. In a fixed reference frame centred

on the Earth this occurs when $v + \varpi + \psi = \pi/2$, where v is the Sun's true anomaly. The distance of the Sun to the Earth at summer solstice is then

$$r_{\text{ss}} = \frac{a(1 - e^2)}{1 + e \sin(\varpi + \psi)}. \quad (10)$$

Thus the precession forcing of the insolation is caused by the term $1 + e \sin(\varpi + \psi)$, which contains the frequencies $|\dot{\psi}_{\oplus} - g_5|$ and $|\dot{\psi}_{\oplus} - g_2|$ with periods 23.7 kyr and 22.5 kyr. These two combine to form the 23 kyr precession frequency mentioned by Milanković (1941).

On Earth the ice ages are probably triggered by changes in the summer insolation at high latitudes on the northern hemisphere (Imbrie, 1982). The typical latitude where this is computed is 65° N, just south of the north polar circle. Investigating the summer insolation at high latitudes makes sense for planets with a low ($\varepsilon \lesssim 30^\circ$) obliquity because there is a steep gradient in insolation with latitude and the ice line is situated at high latitudes. However, for planets with moderate to high obliquity the question arises at which latitude to compute the insolation. A planet with an obliquity of 50° has its polar circles at 40° N and 40° S and its equivalents of the tropics of Cancer and Capricorn are at 50° N and 50° S, meaning the declination of the star travels 100° over the surface of the planet between winter and summer. In addition, planets with high ($\varepsilon \gtrsim 40^\circ$) obliquity have their annual polar insolation close to or exceeding that at the equator. In those cases computing the summer solstice insolation at high latitude makes little sense. An excellent example is given by Mars. Its obliquity oscillates between 15° and 35° (e.g. Ward, 1974), and its polar ice caps disappear and reappear during periods of high and low obliquity respectively (Schorghofer, 2007). The choice of latitude can be avoided by only considering the insolation at the pole and using the orbit-averaged value rather than the summer solstice value.

The yearly polar insolation is given by (Ward, 1974)

$$\langle I_p \rangle = \frac{S_*}{\pi} (1 - e^2)^{-1/2} \sin \varepsilon. \quad (11)$$

where S_* is the stellar flux at the planet's orbit i.e. $S_* = 1361(L_*/L_\odot)(1 \text{ AU}/a)^2 \text{ W m}^{-2}$, L_* and L_\odot are the luminosities of the star and the Sun, ε is the obliquity. Note that equation (11) has no dependence on the precession angle of the planet, ψ , nor the longitude of periastron, ϖ , because of Kepler's second law: the decreased insolation at apastron is balanced by the longer duration.

We want to introduce a few additional quantities. The insolation on planet g determines the overall temperature. Currently we do not know if it has an atmosphere or ocean that is able to transport heat from warmer to colder areas and thus we only study the long-term evolution of the insolation and the black-body equilibrium temperature. The instantaneous black-body equilibrium temperature is given by (e.g. Kaltenegger & Sasselov, 2011)

$$T_{\text{eq}} = T_* \left(\frac{1 - \mathcal{A}}{4\beta} \right)^{1/4} \left(\frac{R_*}{r} \right)^{1/2}, \quad (12)$$

where T_* the star's temperature, \mathcal{A} is the planet's Bond albedo, R_* is the star's radius, r is the planet's instantaneous distance to the star and β represents the fraction of the planet's surface that re-radiates the absorbed flux. For a fast-spinning planet $\beta \sim 1$ while for a tidally locked planet $\beta \sim \frac{1}{2}$. For a planet to remain habitable the black-body equilibrium temperature needs to remain below 270 K (Selsis et al., 2007) to avoid the runaway greenhouse stage. The

orbital average is

$$\begin{aligned} \langle T_{\text{eq}} \rangle &= \frac{2}{\pi} \left(\frac{1 - \mathcal{A}}{\beta} \right)^{1/4} \left(\frac{R_*}{a} \right)^{1/2} \sqrt{1 + e} \mathcal{K} \left(\sqrt{\frac{2e}{1 + e}} \right) \\ &\approx \left(\frac{1 - \mathcal{A}}{\beta} \right)^{1/4} \left(\frac{R_*}{a} \right)^{1/2} \left[1 + \frac{1}{2} \left(\frac{1}{2} e \right)^{1/2} + \frac{25}{16} \left(\frac{1}{2} e \right) \right] \\ &\quad + O(e^{3/2}), \end{aligned} \quad (13)$$

where $\mathcal{K}(k)$ is the complete elliptic integral of the first kind. Note that the equilibrium temperature increases with increasing eccentricity at fixed semi-major axis, just like the annually-averaged insolation, but it does so quicker. It is not clear whether for habitability the instantaneous black-body equilibrium temperature needs to remain below 270 K or the orbitally-averaged one, so we adopt the latter. These relations suggest that the extent of the habitable zone is not only semi-major axis but also also eccentricity dependent. This appears to agree with Williams & Pollard (2002), who suggested that the fundamental quantity for habitability is annually-averaged insolation, and not instantaneous insolation.

The equilibrium temperature of the planet is different from the temperature at the pole that one may derive from the polar insolation, whose annually-averaged value is given by (Schorghofer, 2008)

$$\begin{aligned} \langle T_p \rangle &\approx \frac{1}{2\sqrt{\pi}} \left(\frac{S_*(1 - \mathcal{A}) \sin \varepsilon}{\xi \sigma_{\text{SB}}} \right)^{1/4} (1 - e^2)^{1/8} \frac{\Gamma(\frac{5}{8})}{\Gamma(\frac{9}{8})} \\ &\quad \times \left[1 - \frac{12}{5} \left(\frac{\Gamma(\frac{9}{8})}{\Gamma(\frac{5}{8})} \right)^2 e \sin(\varpi + \psi) \right] + O(e^2), \end{aligned} \quad (14)$$

which has a clear dependence on the longitude of periastron and precession angle of the planet. Here ξ is the infra-red emissivity and σ_{SB} is the Stefan-Boltzmann constant. For Earth $(1 - \mathcal{A})/\xi \sim 1$, which we shall employ later.

In this paper we are interested in planet g and not Earth and below we give an estimate of the periods of the long-term insolation variations on planet g. We can predict what the effect of orbital forcing is on the insolation of planet g. We have $\dot{\psi} = -\alpha \cos \varepsilon$ and so

$$\begin{aligned} \dot{\psi} &= -19.2 \left(\frac{M_*}{M_\odot} \right) \left(\frac{1 \text{ AU}}{a} \right)^3 \left(\frac{24 \text{ h}}{P_r} \right) \left(\frac{m_p}{m_\oplus} \right)^{-0.178} \\ &\quad \times \left(\frac{0.3}{\mathcal{C}} \right) \frac{\cos \varepsilon}{(1 - e^2)^{3/2}} \text{ yr}^{-1}, \end{aligned} \quad (15)$$

where we used $J_2 \propto \frac{R_p^3 \nu^2}{G m_p}$ (Atobe & Ida, 2007; Murray & Dermott, 1999), scaled it from Earth's values, and P_r is the rotation period. This above relation is valid for rotation periods shorter than 13 days. For longer rotation periods the distortion of the planet is no longer only dependent on the rotation and other assumptions will have to be made about J_2 . The value of $\dot{\psi}_g$ is uncertain by a factor of two because of uncertainties in the mass-radius relation, moment of inertia, mass of the planet and star.

Another source of uncertainty in $\dot{\psi}_g$ is the rotation period of planet g. At low eccentricity tidal interaction with the central star should decrease the rotation period on a specific time scale, which when $\nu \gg n$ and $\nu \gg \gamma$ is roughly given by (Ferraz-Mello, 2013)

$$\tau_{\text{gr}} = \frac{16}{45} \left(\frac{\nu}{n} \right)^2 \left(\frac{m_g}{M_*} \right) \left(\frac{a}{R_g} \right)^3 \left(\frac{\gamma}{1 \text{ rad yr}^{-1}} \right)^{-1}. \quad (16)$$

When treating planet g as having internal properties similar to Earth and setting the initial rotation period equal to 1 d we have $\tau_{\text{gr}} \sim 10 \text{ Gyr}$ and thus after 4.5 Gyr the rotation period is less than double the primordial value, but only if the primordial rotation period is shorter than two days. For longer primordial rotation periods the planet will be despun in a shorter time than the age of the system.

Unless it gets trapped in a spin-orbit resonance its rotation rate will be given by the equilibrium rotation (Ferraz-Mello, 2013)

$$\frac{\nu_{\text{lim}}}{n} \approx 1 + 6 \frac{\gamma^2}{n^2} \left(1 + \frac{\gamma^2}{n^2}\right)^{-1} e^2, \quad (17)$$

which works out to be $\nu_{\text{lim},g} \sim 1.26n$ for $e_g \sim 0.22$. When treating planet g as a more solid body such as Mars, the rotation period will have barely changed either. If the planet formed through giant impacts, such as the terrestrial planets of the Solar System (e.g. Kokubo & Ida, 1998), we expect planet g’s rotation to be rapid (Kokubo & Ida, 2007) and to have remained so. All this assumes that there is no large satellite, which modifies the precession and rotation considerably (Brasser et al., 2013).

Assuming for now that planet g’s rotation period is comparable to Earth we have $J_2 \sim 0.71 J_{2\oplus}$ and taking $C = 0.3$, intermediate between Earth and the giant planets, then $\alpha \sim 50''/\text{yr}$. The values of g_6 and s_6 can be read from Table 4. Examining the corresponding eigenvectors in Table 5 and because $M_{i,j} \propto S_{i,j}$, one sees that $M_{6,6} \gg M_{n \neq 6,6}$, so that the eccentricity of planet g remains constant. Hence the obliquity should oscillate with a frequency $|\dot{\psi}_g - s_6|$ where $\dot{\psi}_g = \alpha_g \cos \varepsilon$, and the precession effect should have a frequency of $|\dot{\psi}_g - g_6|$. At low obliquity the periods are roughly 52.2 kyr for the obliquity and 19.4 kyr for precession. These values are likely uncertain by factors of a few but a change in the periodicities does not change the overall outcome. We shall use these expressions in Section 5.

After integrating the motion of the planets and converging to a planar stable solution, the third part of our method concerns the calculation of the annual insolation at the poles. The annual polar insolation depends on the obliquity and eccentricity of the planet; the obliquity forcing depends on the inclination. We only have a planar orbital solution for this system because the relative inclinations are unknown. Thus to compute the obliquity variations we must make an assumption about the inclination distribution. Since most super Earth systems appear to have mutual inclinations less than 5° (Tremaine & Dong, 2012; Figuera et al., 2012), we assume the mutual inclinations of the planets follow a Rayleigh distribution (Fang & Margot, 2012) with a width of $\sigma_i = 2^\circ$. This width corresponds to the current typical mutual inclinations of the planets in the Solar System (Fabrycky et al., 2012) and appears to reproduce the observed inclination distribution of the Kepler super Earth systems (Fang & Margot, 2012). We took the orbital elements of the most stable planar solution and imposed an inclination on each planet. We set the longitude of the nodes to be randomly uniform from 0 to 360° but kept the mean longitudes and longitudes of periastron constant. We generated 100 such configurations and ran them for 1 Myr.

The rotation rate of planet g is mostly unknown, so we assumed a rotation period between 6 h and 240 h. The former is consistent with its expected primordial rotation rate if it formed by giant impacts (Kokubo & Ida, 2007; Kokubo & Genda, 2010) while the latter is an imposed upper limit. The value of J_2 was scaled from that of Earth. When J_2 reaches the value for Venus (4.56×10^{-6}), which occurs when the rotation period is approximately 13 days, we do not lower J_2 beyond this value.

Equations (4) contain no singularities and were integrated numerically using the Bulirsch-Stoer method (Bulirsch & Stoer, 1966) using a pre-generated planetary evolution. We refer to Brasser & Walsh (2011) for further details.

The annual polar insolation and temperature are computed using the obliquity, precession angle, eccentricity and longitude of peri-

astron. The variation in the insolation on long time scales is computed for various initial obliquities and rotation periods.

5 DYNAMICAL STABILITY ANALYSIS

In this section we present our results from numerical simulations. We first discuss the stability analysis, then orbital influence on the climate.

The innermost five planets in the HD 40307 system are closely packed together, with two of them (planets b and e) on fairly eccentric orbits. Planets e and f are in a 3:2 mean motion resonance (Tuomi et al., 2013) thus the stability of the whole system will depend sensitively on whether or not these two planets are actually in resonance. Tuomi et al. (2013) found the system is stable when planets e and f are in a 3:2 resonance and when assuming all the planets are on circular orbits. They determined how the stability of the system depended on the individual initial eccentricity and mean anomaly of each planet but they did not study how the system could be made stable when taking all eccentricities and phases into account. We shall do this below.

When performing a simulation of the nominal system we find that the first two planets to have an encounter are planets e and f and thus they are the bottleneck in any stability study. Hence we shall first investigate the stability of planets e and f.

Laskar (1997) identified that the degree of chaos in a system is directly related to the total angular momentum deficit. Thus, after having analysed planets e and f we proceed to determine how the stability of the system depends on the initial elements of each planet in order of decreasing specific angular momentum deficit. In other words we proceed from highest eccentricity to lowest so that with each step we analyse the then-greatest possible source of chaos/instability.

The following analysis is based on more than 50 000 numerical simulations of the system with different initial conditions. In what follows we aim to find the most stable solution for the subsequent habitability analysis. In those cases where there are large regions of stability we try to keep the solution that yields the lowest χ^2 .

5.1 Planets e and f

We determined how the system’s stability depends on the initial semi-major axis and eccentricity of planet e. The result of this first set of simulations is depicted in Fig. 2. The figure displays the value of D_{max} as a function of initial period ratio with planet f and initial eccentricity of planet e. The graininess of the figure is a result of the sampling resolution and the depth of planetary encounters. High values of D_{max} are mostly the result of one strong encounter rather than many weak ones. Large differences in D_{max} from one pixel to the next becomes a probabilistic argument of whether or not a pair of planets underwent a deep encounter just beyond the Hill sphere during the simulation time. Longer simulations and/or a finer grid could improve smoothness at the expense of much a longer total simulation time to process a single map. This paper is a proof of concept so we leave these additional simulations for a future study.

We also want to stress the following. We approximate the orbital frequencies with the average mean motions via Kepler’s third law. We attempt to measure the stability directly by having the planets undergo encounters. For all of these reasons our stability maps are grainier than those presented in Correia et al. (2005). Returning to Fig. 2, there is only one narrow meta-stable region

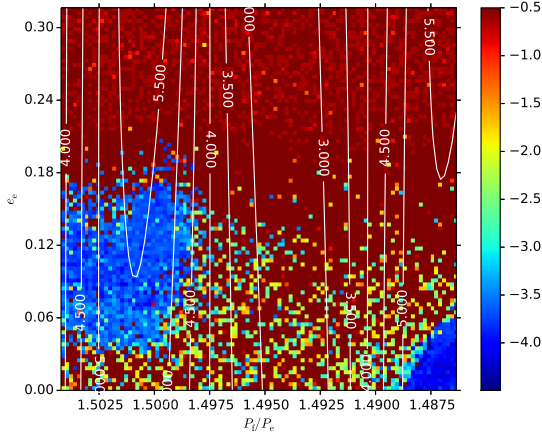


Figure 2. Image map of the maximum diffusion index, D_{\max} . The plot depicts D_{\max} as a function of the initial period ratio P_f/P_e (horizontal axis) and the initial eccentricity e_e (vertical axis). The scale for the colour bar on the right displays the values of D . The contours mark constant values of χ^2 of the goodness of fit between the orbital solution and the radial velocity data.

which is more than 1σ away from the mean. It is at $P_f/P_e < 1.489$ and $e_e \lesssim 0.06$. The lighter blue region around $P_f/P_e \sim 1.5$ and $e_e \sim 0.1$ is unstable on longer time scales and when performing further analysis discussed below. Thus it appears that planets e and f are *not* in a 3:2 mean motion resonance. This claim is in contradiction to that of Tuomi et al. (2013) who stated that the system was only stable if planets e and f are in resonance, and thus this begs further discussion. We can think of two explanations.

First, our initial conditions vary from theirs. Tuomi et al. (2013) did not perform a χ^2 fit to the radial velocity data which we calculated earlier. As a result, our initial longitudes of the planets are different from theirs, and thus the initial resonant angles between planets e and f differ by the same amount. However, when we perform our analysis with the same initial conditions as the nominal solution of Tuomi et al. (2013) we arrive at the same conclusion: the planets e and f are not in resonance. Second, Tuomi et al. (2013) varied the mean motion and initial eccentricity of a single planet while keeping the eccentricities of the others fixed at zero. Varying the mean motion causes variations in the resonant angle and larger changes in χ^2 . With this method it is possible to find a solution where the resonant angle between planets e and f librates. With our initial conditions we were unable to find such a solution that was long-term stable.

We want to investigate further how the stability of the system depends on the remaining parameters. To do so we update the initial period of planet e to be equal to the most stable configuration in the lower-right region of Fig. 2. This requires increasing P_e from 34.62 d to 34.80 d. This is approximately a 2.6σ increase when using the measured standard deviation of the period presented in Table 1. For this stable solution the stability index $D_{\max} = -4.5$ and $\chi^2 = 5.36$. The increase in χ^2 from the nominal solution is caused by the longer orbital period of planet e.

The stable island in the bottom-right corner of Fig. 2 only exists when e_e at lower than its nominal value. Thus the question arises whether a larger stable region, or a more stable configuration, can be found by varying e_e and ω_e , and whether we could simultaneously also lower χ^2 . Thus, we then ran another set

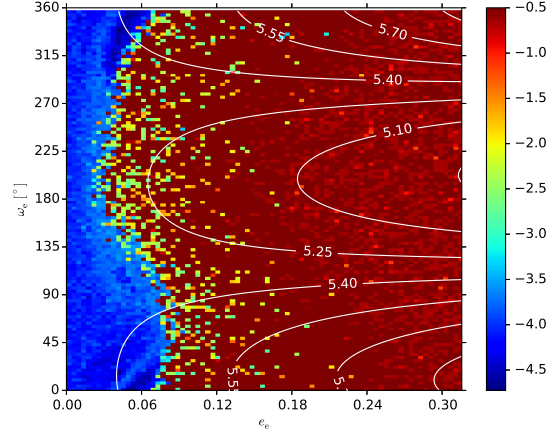


Figure 3. The same as Fig. 2 but this time we varied the eccentricity and argument of periastron of planet e.

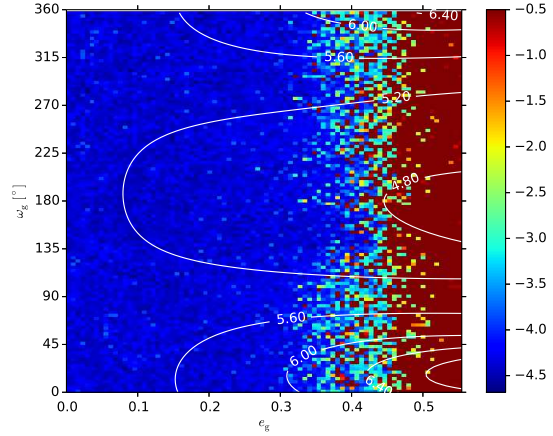


Figure 4. The same as Fig. 2 but this time we varied the eccentricity and argument of periastron of planet g.

of simulations varying the initial eccentricity and argument of periastron of planet e but using the longer orbital period of 34.80 d. The corresponding stability map is depicted in Fig. 3: there is a large region of stable motion when $e_e < 0.05$ for all values of ω_e . From Fig. 3 we found that the most stable solution is at $e_e = 0.033$ and $\omega_e = 312^\circ$. The lowering of the eccentricity is a 1.3σ decrease with χ^2 virtually unchanged from the value obtained from Fig. 2 because χ^2 depends much more sensitively on the period than on the eccentricity.

Here we want to comment on the metastable region in the left part of Fig. 2. When choosing the most stable configuration in the large blue-shaded area and then performing the stability analysis varying e_e and ω_e , we were unable to find a stable region. We performed several additional simulations with somewhat different initial conditions, but our conclusions remained the same. For this reason we are doubtful that planets e and f could be in resonance.

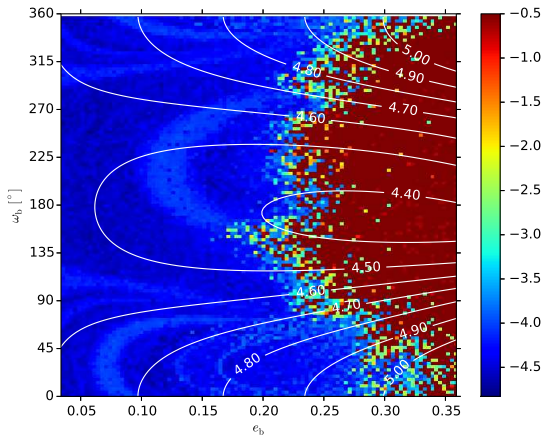


Figure 5. The same as Fig. 2 but this time we varied the eccentricity and argument of periastron of planet b.

5.2 Planets g and b

Now that we have found a stable configuration for the planets e and f the planet with the greatest specific angular momentum is planet g. Tuomi et al. (2013) showed that the stability of the system appears not to depend on the orbit of planet g. We confirm their result. As long as $e_g < 0.4$ the whole system is stable with no dependence on ω_g (see Fig. 4). We only increased ω_g to 183° which coincides with the lowest χ^2 , but left the eccentricity unchanged. We now turn to planet b.

Planets c and d have fairly low eccentricities but planet b does not: its high eccentricity is most likely forced and it is likely in apsidal alignment with planet c. To test this hypothesis we performed additional simulations where we changed the eccentricity and argument of periastron of planet b. The result is depicted in Fig. 5. There is a very large region of stability for $e_b \lesssim 0.2$, with the most stable region occurring when $\omega_b \sim 260^\circ$. In this region $\Delta\varpi_{bc} = \varpi_b - \varpi_c$ librates around 0, corresponding to apsidal alignment between planets b and c (but with a non-zero libration amplitude). Thus, it seems stability is enhanced when one eccentricity mode is damped.

In Fig. 5 the diffusion index shows little variation over a very large region in ω_b and e_b but increases quickly outside it. At low eccentricity there are some lighter blue regions with oxbow shapes. This alternation between more and less stable configurations as a function of ω_b is most likely the result of the nearby 9:4 resonance with planet c (Papaloizou & Trequem, 2010). We focused on those systems for which $D_{\max} < -4.5$ and for which $M_{1,1} \sim 0$ i.e. the eigenmode corresponding to planet b was almost completely damped by tidal forces. We checked the amplitude of the $M_{1,1}$ mode through Fourier analysis using the method of Šidlichovský & Nesvorný (1996) and recorded those cases for which $M_{1,1} \sim 0$. From these criteria we picked the solution with $D_{\max} \sim -4.5$ which has $\omega_b = 228^\circ$ and $e_b = 0.1541$. The eccentricity is approximately 0.8σ lower than the nominal value.

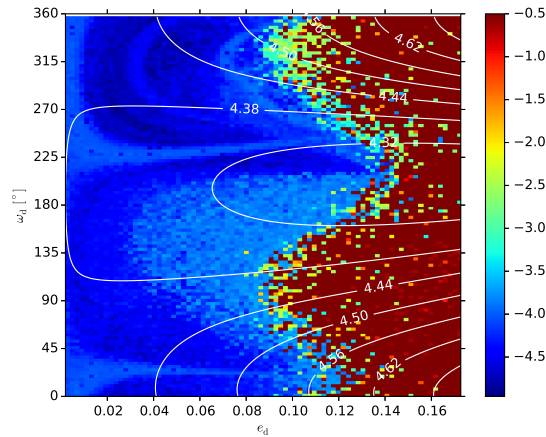


Figure 6. The same as Fig. 2 but this time we varied the eccentricity and argument of periastron of planet d. The current orbital elements of planet d place it in the deep blue region.

and argument of periastron of planet e is mirrored by planet f because of their proximity to resonance. A similar argument applies to planet c: it is most likely locked in apsidal alignment with planet b, and thus changing the eccentricity and argument of periastron of planet c is mirrored by planet b. Last, the stability of the system is only compromised when $e_g > 0.4$ and shows little dependence on its orbital configuration otherwise.

This leaves us with planet d, which is the central and most massive member of the inner five planets. It most strongly influences the dynamics of the other four inner planets. Thus the current orbital elements of planet d are potentially incompatible with the most stable configuration. We have plotted the stability map for planet d in Fig. 6, having changed only e_d and ω_d . The present orbital elements place it in the deep blue, stable region for which $e_d \lesssim 0.12$ and $\omega_d \lesssim 20^\circ$. The most stable region, for which $D_{\max} \sim -5$, occurs for $e_d \lesssim 0.05$ and $225^\circ \lesssim \omega_d \lesssim 360^\circ$. Finally we took the most stable solution in the oxbow shaped region with $e_d = 0.0441$ (0.7σ) and $\omega_d = 249^\circ$. It has $D_{\max} = -4.95$ and $\chi^2 = 4.36$. The total deviation of all changes from the nominal elements is 3.1σ .

We have now converged to a stable solution for the whole system in which planets e and f are close to but not in a 3:2 resonance. Planets b and c are in apsidal alignment because tidal interaction with the host star has damped the amplitude of eigenmode 1. In summary, we now have a fairly complete picture of the dynamics of the HD 40307 system in the planar case. However, is the most stable solution unique? To that end we also analysed the stability of the nominal solution presented by Tuomi et al. (2013), but the maps are not shown because all of these had $\chi^2 \gg 10$. We concluded that the final eccentricities of planets b, e and d are all within 0.8σ of the values reported above, but because the initial mean longitudes of both configurations are not identical, the values of ω for each planet were different. However, given that two different initial conditions approach a similar solution is reassuring and we are certain that we have converged to a stable solution. In the subsection below we explore the stability of the system by imposing a small inclination on the planet’s orbits as outlined in Section 4.

5.3 Planets c and d

We have only analysed the system’s stability by changing the orbits of planets b, e and g. Changing the semi-major axis, eccentricity

5.4 Long-term trends

To determine long-term stability we took the most stable configuration from Fig. 6 and integrated it for 1 Myr with inclined orbits. The procedure to generate the initial conditions is described in Section 4. A long-term stable solution is necessary to obtain the long-term insolation variation on planet g. We ran total of 100 cases and kept those that survived for the full duration.

We also tested these simulations for chaos by performing frequency analysis on the eccentricity eigenfrequencies. We computed the Fourier decomposition of the eccentricity and longitude of periastron of all planets using the method of Šidlichovský & Nesvorný (1996) over eight windows each of length 122 880 yr. For each window we kept the frequency that had the highest amplitude in the spectrum and computed their modified stability index $D' = \log(\sigma_g/g)$, where g is the eccentricity eigenfrequency with the strongest amplitude. A regular system should follow equation (7) and the dominant modes and amplitudes of the Fourier decomposition should stay approximately constant and be clean delta functions (Laskar, 1988). On the other hand, for a chaotic system the dominant frequencies will vary and their peaks will broaden. A multiplet of components can also be viewed as a single component with varying frequency and amplitude, with the frequency of the multiplet being comparable to the frequency spread of the multiplet. In this case the spectral lines associated with some frequencies are not clean delta functions but exhibit a near-Gaussian profile i.e. they have significant sidebands. For a mildly chaotic system the dominant mode will show small variations, such as in the Solar System (Laskar, 1990), but for a strongly chaotic system the dominant mode may be replaced with another mode. This behaviour may occur when two modes have nearly equal amplitudes and the system switches between the two.

We find that 97 systems survive for 1 Myr with 18 having $D'_{\max} < -3$ (lowest -3.5) while the other stable systems have $-2 < D'_{\max} < -0.2$, suggesting that most of these configurations are chaotic, and possibly unstable on longer time scales. The source of the chaos appears to be the alignment of planets b and c, which on long time scales switches between circulation and libration. The planets b and c have strong interaction with planets e and f (Table 5) and perturbations from these planets causes the libration amplitude of $\Delta\varpi_{bc}$ to vary. Sometimes the libration is broken altogether and $\Delta\varpi_{bc}$ circulates. Only at very low eccentricities of the other planets does $\Delta\varpi_{bc}$ librate continuously.

In the next section, we use the output from one of these simulations to compute the long-term insolation variations on planet g. Its evolution is depicted in Fig. 7 and its initial conditions are listed in Table 6. The initial eccentricities and longitudes of periastron were obtained from the stability simulations of Sections 5.1 to 5.3. The values in brackets next to the initial eccentricities are their long-term average and standard deviation. The initial inclinations and longitudes of the ascending node were generated by hand. Their values are indicative only. As one may see: the system is quite stable for at least 1 Myr and most likely for much longer. The Laplace-Lagrange AMD solution yields very similar eigenvectors for the eccentricities but the integration constants C_j^2 are different, and the inclination constants D_j^2 are now non-zero. The total entropy is now $\exp(Z) \sim 5.5$ suggesting 5 eigenmodes out of 11 are activated (eccentricity modes 5 and 6 and inclination modes 1, 3 and 6).

The last question we should answer is whether, on dynamical grounds, we can or cannot rule out the existence of another unseen planet beyond planet g, in particular a gas giant. A rigorous

Table 6. Initial orbital elements of the most stable dynamical solution of the HD 40307 system obtained after a limited dynamical stability study (see Sections 5.1 to 5.3). The inclinations and longitudes of the ascending node are inserted by hand as described in Section 4 and are indicative only. The masses and mean anomalies have been left unchanged from Table 1. The bracketed values in the eccentricity row denote their long-term average values and standard deviations.

Parameter	HD 40307 b	HD 40307 c	HD 40307 d
P [days]	4.3122	9.6183	20.4314
e	0.1541 [0.085,0.034]	0.05778 [0.063,0.023]	0.04408 [0.044,0.020]
i [°]	1.85	1.49	0.26
Ω [°]	254.4	223.5	102.7
ϖ [°]	228.0	234.9	249.0
λ [°]	150.0	5.0	353.0
a [AU]	0.047524	0.08113	0.13407
	HD 40307 e	HD 40307 f	HD 40307 g
P [days]	34.8062	51.7768	196.3429
e	0.03279 [0.047,0.022]	0.03000 [0.058,0.025]	0.2205 [0.22,0.001]
i [°]	0.82	0.43	0.97
Ω [°]	220.1	244.6	187.3
ϖ [°]	312.0	355.0	183.0
λ [°]	62.0	23.8	128.0
a [AU]	0.1912	0.2491	0.6069
$\chi^2 = 4.7$			

dynamical test of this hypothesis is beyond the scope of the paper. However, we performed two simple tests: one in which we placed a Saturn-mass planet on a circular orbit at 0.9 AU i.e. just 0.3 AU away from planet g. In the second we placed a Saturn-mass planet at 1.7 AU with an eccentricity of 0.3. In the first case the eccentricity of planet g stays approximately constant. In the second case the eccentricity of planet g oscillates between 0 and 0.22 with a period of about 20 kyr. In both cases the eccentricity of the hypothetical Saturn-mass planet remains constant and the inner five planets remain unaffected. Thus, it appears that the system is fairly resistant to there being another, external planet. The existence of an external, eccentric gas giant could explain planet g's eccentricity because it could be near the maximum of its eccentricity cycle. The high eccentricity of the gas giant farther out could be the result of previous planet-planet interactions (e.g. Juric & Tremaine, 2008). Unfortunately, it seems unlikely to rule out the existence of another planet on dynamical grounds alone, but observations indicate that it is unlikely such a planet exists (Tuomi et al., 2013). A planet more massive than $10 M_{\oplus}$ up to 2 AU distance is definitely ruled out, but a 10-20 M_{\oplus} object at 3 AU cannot be ruled out at this stage (Tuomi et al., 2013). However, as stated above, the existence of such a planet or a gas giant at larger distance appears to have little effect on the dynamics of the system and the habitability of planet g unless the nodal regression of one of these planets happens to resonate with $\dot{\psi}_g$.

6 OBLIQUITY AND INSOLATION EVOLUTION

In this section we produce maps of the obliquity range, precession frequency, insolation and other quantities on planet g. The methods were described in Sections 3 and 4: we take the output from a stable configuration that was integrated for 1 Myr and used as input to numerically integrate the equations of the obliquity and precession

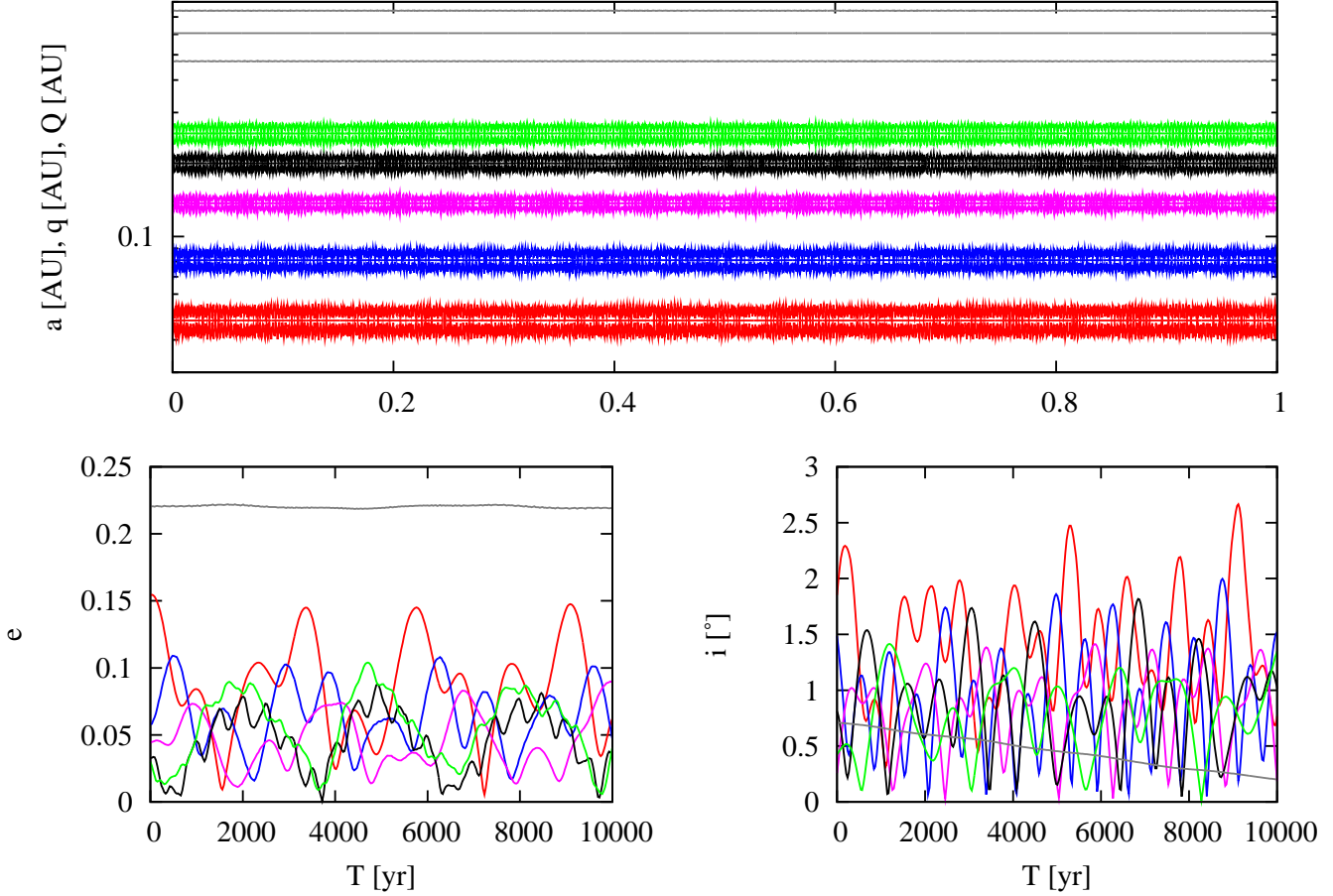


Figure 7. Evolution of the HD 40307 system for 1 Myr. The top panel shows the periastron, semi-major axis and apastron distance of all planets. The colours are red for planet b, blue for planet c, magenta for planet d, black for planet e, green for planet f and grey for planet g. The bottom left panel shows the eccentricity evolution for the first 10 kyr and the bottom right panel depicts the inclinations.

evolution. We have no prior knowledge of the rotation rate of planet g nor its J_2 moment, so we decided to scale these from Earth’s values assuming that the fluid Love numbers are the same. We set J_2 equal to Venus’ value for rotation periods longer than 13 days.

6.1 Obliquity evolution

We display the magnitude of the obliquity oscillations as a function of rotation period and initial obliquity in Fig. 8. For rotation periods shorter than 1.5 days, longer than 2 days and low obliquities, the oscillation amplitude is generally small i.e. less than 5° . The oscillation period is generally of the order of 20 kyr or longer. A similar evolution is observed at long rotation periods and high obliquities. However, the situation changes dramatically in a narrow band originating from (0.25, 85) and reaching all the way down to (1.5, 0). Here the precession of the spin pole of planet g is in resonance with the s_6 inclination eigenfrequency i.e. $\dot{\psi}_g = s_6$, and the planet is in a Cassini state (Colombo, 1966), specifically Cassini state 2. Inside Cassini state 2 the obliquity oscillates with large amplitude. For obliquities close to zero, the planet is in Cassini state 1, such as Mercury (e.g. Correia & Laskar, 2010). For planet g the only substantial forcing on the obliquity is caused by the $N_{6,6}$ term (which is the free inclination i_f). For Fig. 8 it was $i_f = 0.58^\circ$. The obliq-

uity at which the states occur are approximately given by (Ward & Hamilton, 2004)

$$\varepsilon \approx \arctan\left(\frac{\sin i_f}{1 \pm \alpha/s_6}\right), \quad \varepsilon \approx \pm \arccos\left(\frac{s_6 \cos i_f}{\alpha}\right). \quad (18)$$

The first two roots correspond to states 1 and 3 (state 3 is retrograde), while the second formula approximates states 2 and 4. Note that states 1 and 4 do not exist when $\alpha/s_6 < (\sin^{2/3} i_f + \cos^{2/3} i_f)^{3/2} \approx 1.07$, corresponding to $\alpha = 31.5''/\text{yr}$, with a matching critical obliquity $\tan \varepsilon_c = \tan^{1/3} i_f$ i.e. $\varepsilon_c \approx 12.2^\circ$. For the parameters we chose states 1 and 4 disappear when the rotation period is nearly 1.5 days, which matches Fig. 8 above.

6.2 Polar insolation and black-body temperature

How do these variations in obliquity affect the yearly insolation and temperature at the poles? We display the results in the following figures. In the top-left panel of Fig. 9 we display the average yearly insolation in Watts per square metre at the North pole as a function of the rotation period (horizontal) and initial obliquity (vertical). The initial precession angle was set to $\psi = 90^\circ$. The scale is displayed by the vertical bar. The region where large excursions in the obliquity occur are mirrored in this figure. The top-right

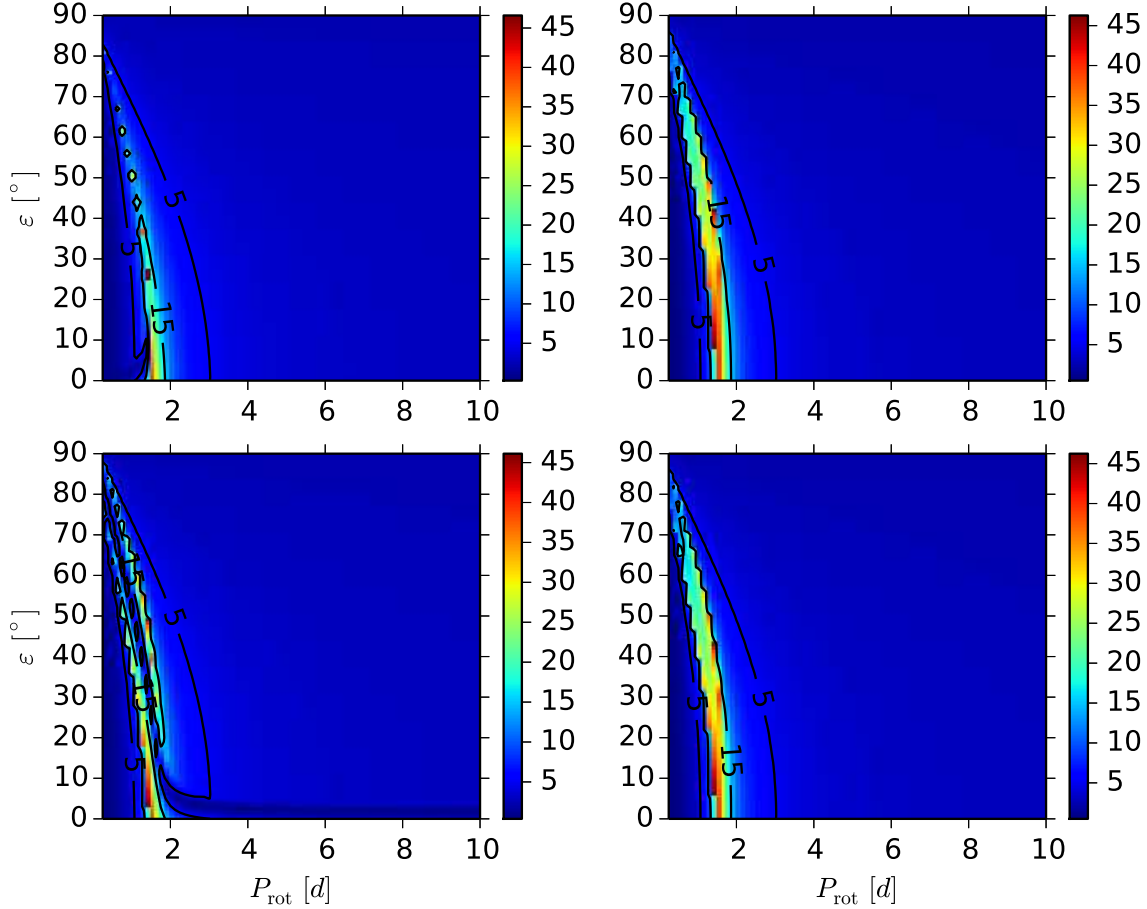


Figure 8. Contours of the amplitude of the obliquity oscillations as a function of rotation period and initial obliquity. The four panels are for initial precession angles of 0°, 90°, 180° and 270° going clockwise from the top left. Note the two distinct resonances when $\psi = 180^\circ$.

panel shows contours of the standard deviation of the insolation at the North pole. These contours follow those of the obliquity: the yearly-averaged insolation only depends on the obliquity. The bottom-left panel displays the average black-body temperature at the North pole in Kelvin obtained from equation (14), while the bottom-right shows the standard deviation of the black-body temperature range. Thus for obliquities above 30°, the average North pole black-body temperature is between 125 K and 150 K but the standard deviation of the long-term temperature range is about 20 K, so the expected long-term peak-to-peak changes could have amplitudes of up to 50 K. The long-term insolation variations are ~ 20 W unless the planet is in the Cassini state.

How does the insolation and black-body temperature on planet g compare to Earth's? We created a plot of the yearly insolation at the North pole for planet g and Earth (top row) and their black-body temperatures (bottom row). We fixed the initial obliquity of planet g at 25°. The rotation period was 3 d for the left column and 1.5 d for the middle column, inside the Cassini state.

In the first case, the amplitude of the insolation variation is comparable to that of Earth, but the periodicities are very different: for Earth the dominant periodicity is 41 kyr, with modulations of 39 kyr and 53 kyr, while for planet g the period is approximately 102 kyr

(frequency $|\dot{\psi}_g - s_6| \sim 12.7''/\text{yr}$). The situation is different for the evolution of the black-body temperature: the periodicity for planet g is 40 kyr caused by precession (frequency $|\dot{\psi}_g - g_6| \sim 32.0''/\text{yr}$), with the 102 kyr modulation on top. For the Earth the precession component is 23 kyr, modulated by obliquity at 41 kyr. However, there is a striking difference between the left top and bottom panels. While for both planet g and Earth the annual average polar insolation is similar and shows little variation, the same cannot be said for the polar black-body temperature. For Earth this shows a 10 K variation on long time scales – seasonal variations are not taken into account – but for planet g the range is 50 K! If Earth's 10 K variations can cause regular ice ages, the effect on planet g appears much more enhanced and would likely occur on a similar time scale. The insolation variation on planet g is substantially different from Earth's because of its high eccentricity. Indeed, the temperature deviations are mostly precession driven, while for Earth these are driven both by precession and obliquity because the amplitude of eccentricity oscillations is not much larger than the obliquity oscillations.

When the rotation period of planet g is 1.5 d and the planet is in the Cassini state, the situation is changed dramatically: its obliquity oscillates with a large ($\sim 25^\circ$) amplitude and period 450 kyr. The polar insolation now varies by a factor of 10 and the polar black-body temperature variations are also much larger. The short-

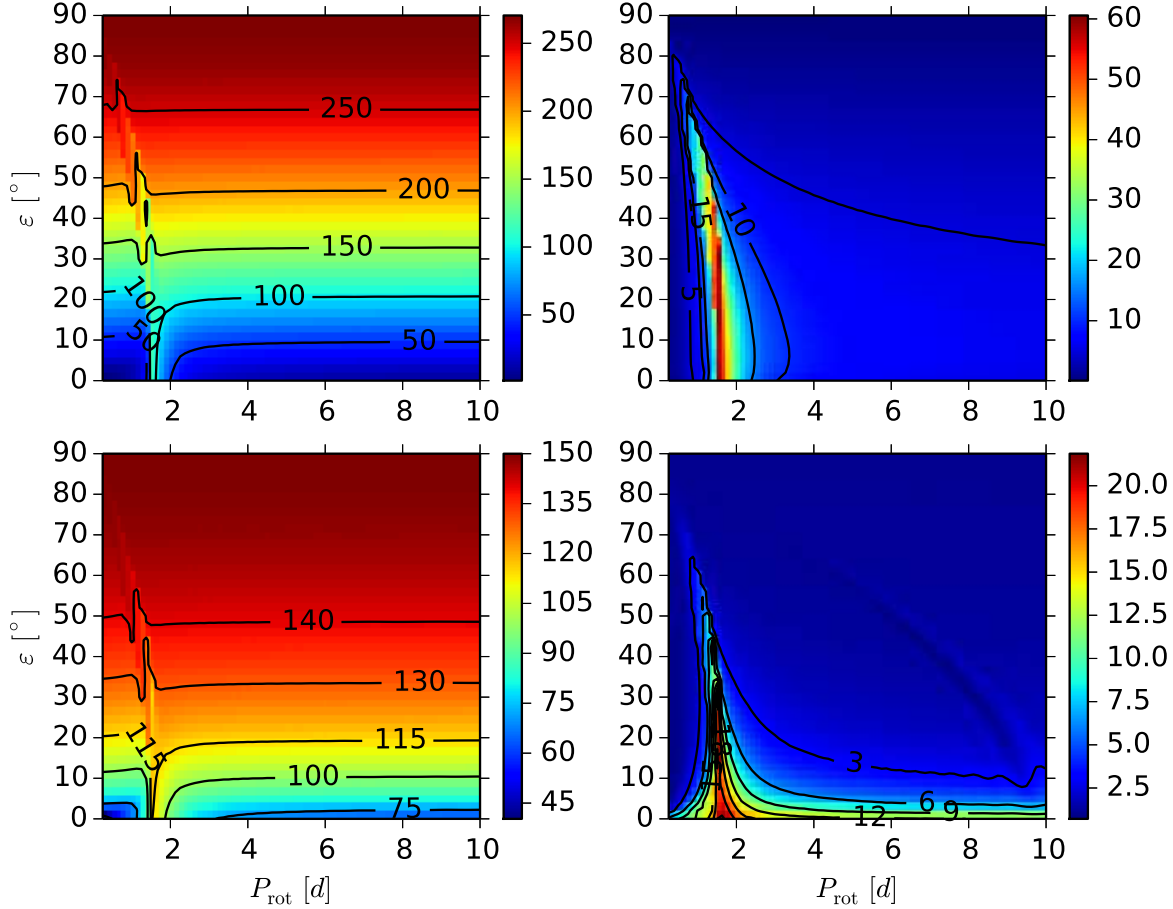


Figure 9. The variations in polar insolation (top left) and its standard deviation (top right) as a function of rotation period and obliquity. The bottom left panel depicts the variation in polar black body temperature while the bottom right panel shows its standard deviation.

period variations are caused by the precession, as they were in the 3 d rotation case, but the long-periodic variation is caused by the obliquity. The largest difference with the 3 d rotation case is the long-term variation in the polar insolation. If the climate change is primarily driven by changes in polar insolation rather than temperature variations then the 1.5 d rotation case could cause more extreme climate variations. As we argued in Section 4, during periods of high obliquity the equator becomes colder than the pole, which could cause a dramatic shift in ice deposits from the poles to the equator (as happens on Mars; Schorghofer, 2007). In addition, the high-obliquity causes the polar circles to be near the equator and the tropics of ‘Cancer’ and ‘Capricorn’ to be near the pole, causing rapid and extreme seasonal temperature variations. Once again taking Mars as an example, its extreme obliquity variations inhibit the climate’s stability because of the melting and freezing of the polar caps, and the exchange of ice between the poles and the equator (Schorghofer, 2007). Thus we cautiously argue against the 1.5 d case being suitable for habitability unless the planet happens to be at the exact Cassini state equilibrium where the obliquity is constant.

So far we have only analysed the variation in insolation for a rotation period of 3 d and 1.5 d i.e. outside and inside the Cassini state. There is also a domain of shorter rotation periods. For these

shorter rotation periods the climate cycles occur at a faster pace. For example, when the rotation period is just 12 h the precession periodicity approaches 10 kyr and the obliquity variations occur on a time scale of 20 kyr.

7 DISCUSSION

In the previous sections we analysed the dynamical stability of the HD 40307 super Earth system using numerical methods. We followed this up with a detailed dynamical study on the precession, obliquity and insolation variations on planet g. Several of our results require further elaboration.

First we discuss our methods. In this study we did not vary the masses of the planets for two reasons. First, changing the masses would have added an extra dimension to our numerical simulations and the parameter space would have pushed the limits of our computational resources. Second, the stability of the system depends on a low power of the planetary masses (Chambers, 1996; see Section 2). The only quantity that depends linear on the masses are the precession frequencies. The uncertainty in the masses are less than factors of two and thus these quantities change by a similar amount. Similarly, it has been estimated that the $\sin I$

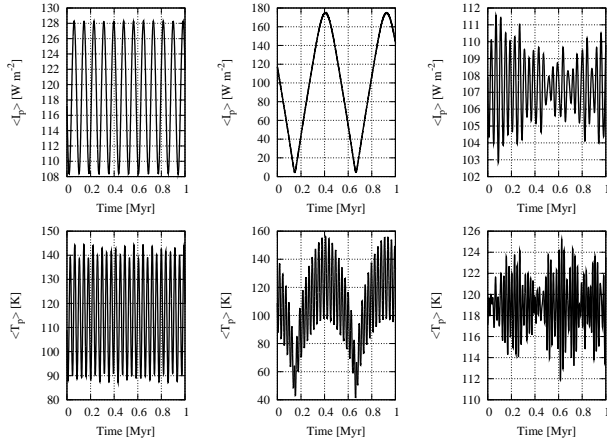


Figure 10. The evolution of the annually-averaged polar insolation of planet g for a 3 d rotation period (top left), 1.5 d rotation period (top middle) and Earth (top right), and the polar black-body temperature (bottom left, middle and right).

effect typically increases the masses by an amount lower than 20% (Tremaine & Dong, 2012), which is also not enough to cause substantial changes in the dynamics. Thus we decided to use the nominal masses for this study.

The next topic pertains to the inclinations of the planets. The RV data typically are unable to constrain the mutual inclinations of the system, unless it has reached a fixed point through tides (Batygin & Laughlin, 2011). That is likely not the case here, so we introduced the inclinations by hand as explained in Section 4 based on the method of Fang & Margot (2012). They demonstrated that their Rayleigh distribution matched well with the Kepler super Earth systems. We could have chosen to use a different distribution which would probably have worked just as well, but this choice would have required additional justification. We caution against increasing the maximum inclination much above $\sim 5^\circ$, because this would violate constraints that we have from planet formation theories. It would also add a substantial amount of Angular Momentum Deficit to the system which could be exchanged with eccentricity and ultimately make the system less stable (Laskar, 1997).

The possible presence of additional planets also requires some elaboration. As we said in Section 5 a Saturn-mass planet on an eccentric orbit within 2 AU of the star is able to significantly perturb planet g. A low-eccentricity Saturn-mass planet will have little to no effect. But what about other planets beyond 3 AU, especially gas giants just like in our Solar System? The distant spacing of such gas giant planets would cause them to have little dynamical effect on planet g and the planets inside of it, unless one of the eigenfrequencies of these hypothetical gas giants is commensurate with g_6 (or s_6). Such a secular resonance would increase planet g’s eccentricity to a high value and could make it cross the orbits of the inner 5 planets. This would require a coincidence between the eigenfrequencies which is unlikely to be the case. Thus we suggest that the addition of gas giant planets beyond 3 AU does not pose a large risk to the dynamical stability of planet g and the innermost planets.

The next issue that warrants discussion is the uncertainties in the parameters. The largest uncertainties are in the radius and rotation period of planet g. Both of these directly affect the precession period. Increasing the precession period by a factor of two implies an increase in the planetary radius by 25%, larger than the errors

presented in Sotin et al. (2007). Concerning the rotation period, we have demonstrated in Section 2 that if planet g formed rotating quickly, it will have most likely remained so. Only if it formed with a long rotation period could it be despun. Thus our estimates of a factor of two uncertainty in $\dot{\psi}_g$ is probable. Increasing $\dot{\psi}_g$ by a factor of two lowers the precession and obliquity oscillation periods by a similar amount, reducing them from 40 kyr to 20 kyr and from 102 kyr to 51 kyr at a 3 d rotation period. All of these are comparable to Earth’s forcing frequencies and our conclusions remain the same.

We now turn to the habitability of planet g. Due to a lack of information about its interior and exterior we made certain assumptions, based on recent results in the literature, about how the planet’s obliquity would respond to orbital forcing. With no knowledge about oceans or the atmosphere we can only investigate the long-term behaviour of the insolation and black-body temperature at a given latitude, either their yearly-averaged values or those at summer solstice and compare them with Earth’s. For mathematical simplicity we took the values at the north pole. We find that the high eccentricity and quick precession of planet g because of its proximity to the star cause substantial changes in polar black-body temperature on a time scale of up to a few tens of thousands of years. For rotation periods of 1.5 days the obliquity displays large-amplitude oscillations with long period which also dramatically affect the climate.

A third question pertains to what our results imply. Using the nominal eccentricity of planet g, and reasonable assumptions about its J_2 moment, outside of the Cassini state its axial precession is comparable to Earth’s and the polar black-body temperature varies on time scales of ~ 40 kyr if the rotation period is a few days, and shorter time scales for a shorter rotation period. Given that the magnitude of these black-body temperature variations are much larger than Earth’s, we speculate that this causes equally drastic but periodic changes in the climate, with the polar regions being affected much more strongly than the tropics. The most likely consequences depend on the planet’s geography and atmosphere. For a dry planet such as Mars, assuming a thin atmosphere, the most severe effect is the reappearance and disappearance of the polar ice caps and high and low obliquity. For an ocean planet a similar effect may occur. It has been suggested that for planet g to have a temperature similar to Earth’s it requires a 10 bar carbon dioxide atmosphere (Tian, 2013). Such a thick atmosphere would most likely buffet the insolation variations induced by planetary perturbations because it has much more efficient heat transport than Earth’s thin atmosphere.

8 SUMMARY AND CONCLUSIONS

We investigated the dynamical stability of the HD 40307 planetary system with the aid of numerical simulations. Once a stable solution was found it was used to determine the long-term insolation variation of planet g, which is situated in the habitable zone of the star. We found that the most stable orbital solution of the whole system requires a 2.6σ increase in the period of planet e. This places planet e outside of a 3:2 mean-motion resonance with planet f. It further requires a reduction in its eccentricity of 1.3σ .

The high eccentricity of planet b is the result of forcing from the other planets, mostly from planet c. Its own eccentricity eigenmode is most likely damped by tides and thus it is in apsidal alignment with planet c. The most stable configuration of the system requires

some further reduction in the eccentricities of planets b and d. It is 3.1σ from the nominal solution with a reduced $\chi^2 = 4.36$.

The Milanković cycles on planet g manifest themselves with a period similar to those on Earth, but the polar black-body temperature variations are much more intense than on Earth because of planet g's high eccentricity. For this reason we cautiously conclude that planet g may not be very habitable at high latitudes when the obliquity is low, thereby reducing its overall habitability. The high eccentricity could cause regular, intense ice ages and severe ocean level changes on a wet planet such as Earth and regular disappearance and reappearance of dry polar ice caps such as on Mars. While the periodicities are uncertain by factors of a few, the variation in the insolation is not and thus the overall conclusion remains the same. If planet g formed with a fast rotation through a giant impact stage, the rotation likely would have remained fast, causing rapid precession and short periods between ice ages, as well as reducing heat transport from warmer to cooler regions (Williams, 1988).

9 ACKNOWLEDGEMENTS

We thank Mikko Tuomi for stimulating discussions and for sharing the HARPS-TERRA radial velocity data of HD 40307. We thank Sylvio Ferraz-Mello for discussions and the sharing of software to compare the simulations and the radial velocity data. Last, and most importantly, we are deeply grateful to a tough and fair anonymous reviewer for his/her patience and very valuable feedback that improved this work substantially. RB thanks SI and EK for their hospitality during several trips to Tokyo. The Condor Software Program (HTCondor) was developed by the Condor Team at the Computer Sciences Department of the University of Wisconsin-Madison. All rights, title, and interest in HTCondor are owned by the Condor Team.

10 BIBLIOGRAPHY

- Abe-Ouchi A., Saito F., Kawamura K., Raymo M. E., Okuno J., Takahashi K., Blatter H., Nature 500, 193.
- Agnor C. B., Lin D. N. C., 2012, ApJ, 745, 143
- Anglada-Escudé G., Butler R. P., 2012, ApJS, 200, 15
- Atobe K., Ida S., Ito T., 2004, Icar, 168, 223
- Atobe K., Ida S., 2007, Icar 188, 1
- Batalha N. M., et al., 2013, ApJS, 204, 24
- Batygin K., Laughlin G., 2011, ApJ, 730, 95
- Batygin K., Morbidelli A., 2013, AJ, 145, 1
- Beaugé C., Ferraz-Mello S., Michtchenko T. A., 2012, RAA, 12, 1044
- Borucki W. J., et al., 2011, ApJ, 728, 117
- Brasser R., Walsh K. J., 2011, Icar, 213, 423
- Brasser R., Ida S., Kokubo E., 2013, MNRAS, 110
- Brouwer, D., van Woerkom, A. J. J. 1950. Astron. Papers Amer. Ephem. 13, 81-107.
- Bulirsch, R., Stoer, J. 1966. Numerische Mathematik 8, 1-13.
- Chambers J. E., Wetherill G. W., Boss A. P., 1996, Icar, 119, 261
- Chambers J. E., 2001, Icar, 152, 205
- Chiang E., Laughlin G., 2013, MNRAS, 431, 3444
- Colombo G., 1966, AJ, 71, 891
- Correia A. C. M., et al., 2005, A&A, 440, 751
- Correia A. C. M., Laskar J., 2010, Icar, 205, 338
- Fabrycky D. C., et al., 2012, arXiv:1202.6328
- Fang J., Margot J.-L., 2012, ApJ, 761, 92
- Ferraz-Mello S., 2013, CeMDA, 116, 109
- Figueira P., et al., 2012, A&A, 541, A139
- Gaidos E., Fischer D. A., Mann A. W., Lépine S., 2012, ApJ, 746, 36
- Hansen B. M. S., Murray N., 2012, ApJ, 751, 158
- Howard A. W., et al., 2010, Sci, 330, 653
- Howard A. W., et al., 2012, ApJS, 201, 15
- Huybers, P., Wunsch, C., 2005, Nature 434, 491
- Huybers, P., 2011, Nature 480, 229
- Ida S., Lin D. N. C., 2010, ApJ, 719, 810
- Imbrie J., Imbrie J. Z., 1980, Sci, 207, 943
- Imbrie J., 1982, Icar, 50, 408
- Jurić M., Tremaine S., 2008, ApJ, 686, 603
- Kaltenegger L., Sasselov D., 2011, ApJ, 736, L25
- Kasting J. F., Whitmire D. P., Reynolds R. T., 1993, Icar, 101, 108
- Kley W., Nelson R. P., 2012, ARA&A, 50, 211
- Kokubo E., Ida S., 1998, Icar, 131, 171
- Kokubo E., Ida S., 2007, ApJ, 671, 2082
- Kokubo E., Genda H., 2010, ApJ, 714, L21
- Laskar J., 1988, A&A, 198, 341
- Laskar J., 1990, Icar, 88, 266
- Laskar J., 1993, CeMDA, 56, 191
- Laskar J., et al., 1993, A&A, 270, 522
- Laskar J., 1997, A&A, 317, L75
- Levison H. F., Duncan M. J., 1994, Icar, 108, 18
- Lissauer J. J., et al., 2011, ApJS, 197, 8
- Lithwick Y., Wu Y., 2012, ApJ, 756, L11
- Lopez E. D., Fortney J. J., Miller N., 2012, ApJ, 761, 59
- Lovis C., et al., 2011, A&A, 528, A112
- McGehee, R., Lehman, C., 2012, SIAM J. Appl. Dyn. Syst. 11, 684707
- Marzari F., Tricarico P., Scholl H., 2003, MNRAS, 345, 1091
- Mayor M., Queloz D., 1995, Natur, 378, 355
- Mayor M., et al., 2003, Msngr, 114, 20
- Mayor M., et al., 2009, A&A, 493, 639
- Mayor M., et al., 2011, arXiv, arXiv:1109.2497
- Michtchenko T. A., Malhotra R., 2004, Icar, 168, 237
- Milanković, M., 1941. Royal Serbian Sciences 33,633
- Morbidelli A., Brasser R., Tsiganis K., Gomes R., Levison H. F., 2009, A&A, 507, 1041
- Neron de Surgy, O., Laskar, J., 1997, A&A 318, 975
- Nobili A., Roxburgh I. W., 1986, IAUS, 114, 105
- Papaloizou J. C. B., Terquem C., 2010, MNRAS, 405, 573
- Petrovich C., Malhotra R., Tremaine S., 2013, ApJ, 770, 24
- Raymond S. N., Barnes R., Mandell A. M., 2008, MNRAS, 384, 663
- Rein H., 2012, MNRAS, 427, L21
- Saha P., Tremaine S., 1994, AJ, 108, 1962
- Schorghofer N., 2007, Natur, 449, 192
- Schorghofer N., 2008, GeoRL, 35, 18201
- Selsis F., Kasting J. F., Levrard B., Paillet J., Ribas I., Delfosse X., 2007, A&A, 476, 1373
- Šidlichovský M., Nesvorný D., 1996, CeMDA, 65, 137
- Sotin C., Grasset O., Mocquet A., 2007, Icar, 191, 337
- Tian, F., 2013, Science China, Earth Sciences, 56, 1
- Tremaine S., Dong S., 2012, AJ 143, 94
- Tuomi M., Anglada-Escudé G., Gerlach E., Jones H. R. A., Reiners A., Rivera E. J., Vogt S. S., Butler R. P., 2013, A&A, 549, A48
- Valencia D., O'Connell R. J., Sasselov D., 2006, Icar, 181, 545
- Ward, W. R., 1974, JGR, 79, 3375
- Ward W. R., Hamilton D. P., 2004, AJ, 128, 2501
- Williams D. M., Kasting J. F., 1997, Icar 129, 254
- Williams D. M., Pollard D., 2003, IJAsB, 2, 1
- Williams G. P., 1988, CIDy, 3, 45
- Wisdom J., Holman M., 1991, AJ, 102, 1528
- Wu Y., Lithwick Y., 2011, ApJ, 735, 109